Design of a Novel Converter Between Li-Ion Battery and Supercapacitor to Feed Synthetic Aperture Radar Loads for Satellite Applications

Gencer Tulay*‡, İres İskender**

* Electrical Electronics Engineering Department, Engineering Faculty, Gazi University, Ankara, Turkey

**Electrical Electronics Engineering Department, Engineering Faculty, Çankaya University, Ankara, Turkey

(ismailgencer.tulay@gazi.edu.tr, ires@cankaya.edu.tr)

‡ Corresponding Author; First Author, Electrical Electronics Engineering Department, Engineering Faculty, Gazi University, Ankara, Turkey, Tel: +90 312 210 1310, ismailgencer.tulay@gazi.edu.tr

Received: 30.10.2020 Accepted:30.11.2020

Abstract- For satellite applications the active duty life of a satellite depends mainly on the battery lifespan. The charging or discharging current has an important role in useful life of batteries. For this purpose, the converters used in power supplies including batteries should be accurately designed such that the large current of batteries can be prevented. The power converter proposed in this paper is used to transfer energy from battery to supercapacitor when SAR (Synthetic Aperture Radar) load is active. Accordingly, the lifespan of battery and hence the lifespan of satellite will be extended. Parallel to preventing the large discharging current of batteries the proposed converter has another important property such that it is able to vary the input voltage without having any stability problems. The operating performance of the converter that is composed of Weinberg and Buck converters is analyzed using PSpice software and the results of simulations are verified through experiments. The results show that how well the converter operates satisfying the conditions required for satellite applications.

Keywords Supercapacitor, Weinberg converter, Buck converter, satellite power subsystem.

1. Introduction

Radar stands for detection and determination of range by the help of radio waves. The wave signal produced by radar antenna is sent to target and then is backscattered and received by a receiver. Radar signal is generated by a high frequency generator and the backscattered signal is received by a sensitive receiver. The most important feature of a radar device is to determine the range on time spent basis [1, 2].

Batteries have been using as energy storage device for a lot of different applications [3-7]. Li-Ion battery is a rechargeable energy storage device used in satellite power subsystems. The battery is charged from photovoltaic array, and then delivers its energy to the load on demand. Currently, the lithium ion batteries are massively used in satellites rather than those with nickel cadmium cells. This is due the properties of lithium ion battery which has higher cell voltage level about three times, higher energy density, lower self-discharging, longer cycle life, extensive temperature range and without suffering from memory effect. The lifespan of the satellite depends on the lifespan of the battery on a large scale for satellite applications [8].

Similar to batteries, supercapacitors have the property of charging and discharging energy. The main advantage of supercapacitors is that their power density is much higher than that of batteries for a short duration. Supercapacitors lose about 15% of their charge per day due to self-discharging property, so they are not well-suited for long-term energy storage. Batteries have advantage of long period energy storage while supercapacitors are preferred for higher instantaneous power [9].

The payloads and satellite subsystems are feeding by the regulated output of Li-Ion battery in traditional architecture. In satellites including SAR payload, battery's life is shortened when high pulse currents are drawn for instantaneous high power applications. Supercapacitors cannot be replaced by batteries but they can be used as a complementary energy storage device for satellite applications. The usage of supercapacitors in hybrid power systems extends the battery's life by mitigating the peak power duties from batteries and this makes the combination of supercapacitor and battery as a hybrid system to be a perfect approach for satellite applications. The block diagram shown in Fig.1 shows a similar architecture as given in [10]

and is corresponding for power supply alternatives for electrification of settlements.

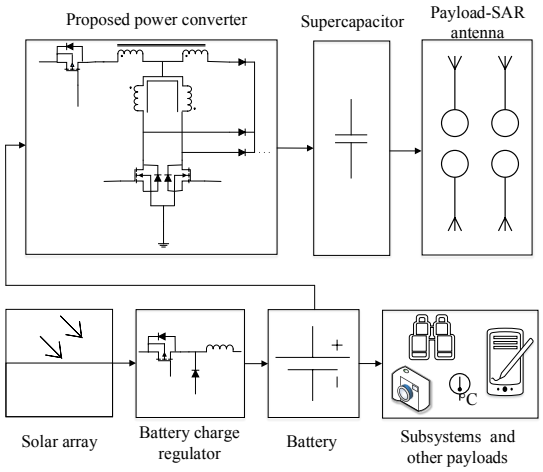

Fig. 1. Block diagram of the proposed architecture.

Supercapacitor voltage may be higher or lower than the battery voltage depending on the solar panel voltage and the supercapacitor voltage right after feeding the SAR load. The supercapacitor voltage can be adjusted to the required level by the hybrid converter including Weinberg (step up) and buck converter (step down).

There are different studies in literature in which Weinberg converter and its operating properties have been analyzed [11-15]. Buck converter is a simple dc-dc converter used in application to decrease the dc voltage [16-20].

The combination of Weinberg and Buck converters used in this study can be analyzed considering performance parameters as efficiency, power density, duty life and cost of the satellite in the scope of space applications.

The simplicity of the converters and their operating stability are important and should be considered in designing converters used in satellite applications [21, 22]. The Weinberg converter given in [12] is able to vary the voltage, but from the view point of stability it has disadvantage as having a right half plane zero which makes it impossible to be used in satellite applications [23, 24]. There are studies in literature in which bidirectional Weinberg converter [13] and bidirectional Buck converter [20] are studied. These converters are not suitable to be used in the converter proposed in this study considering the unidirectional property of the power transfer. The proposed converter has the advantages of decreasing or increasing the voltage level, unidirectional power transfer property and stability for different operating modes.

The supercapacitor is fed from the battery through the proposed unidirectional power converter. In this study the supercapacitor voltage is considered to be 50 V and the converter performance is analyzed to fix this voltage for different voltage level of battery which may be between 40 and 60 V.

The working principle and related equations of the proposed converter are presented in Section 2. The results of the study and the related discussions are examined in Section 3 and the conclusion of the study is given in Section 4.

2. Working Principles of the Proposed Converter

The converter proposed in this study is composed of Weinberg and Buck converters. Using the transfer function of system shows that the hybrid converter has no right half plane zero ensuring the stability of the hybrid system. Though the Weinberg and Buck converters have been used separately for the satellite applications, the proposed converter is a hybrid type and combines their advantages. Weinberg and Buck converters are shown in Fig.2-a and Fig.2-b, respectively.

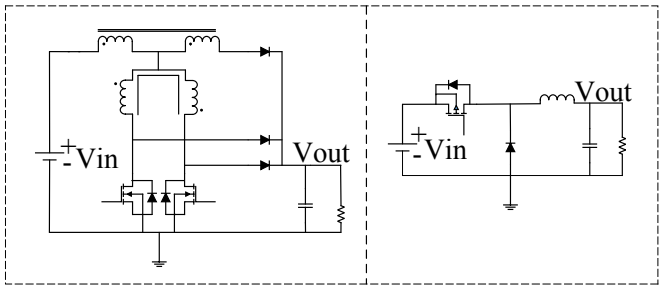

Fig. 2-a. Weinberg converter, **Fig. 2-b.** Buck converter

There is a switch between the input source and the inductor L_1 representing the difference between the proposed converter and classical Weinberg converter. The configuration of the proposed converter is shown in Fig.3.

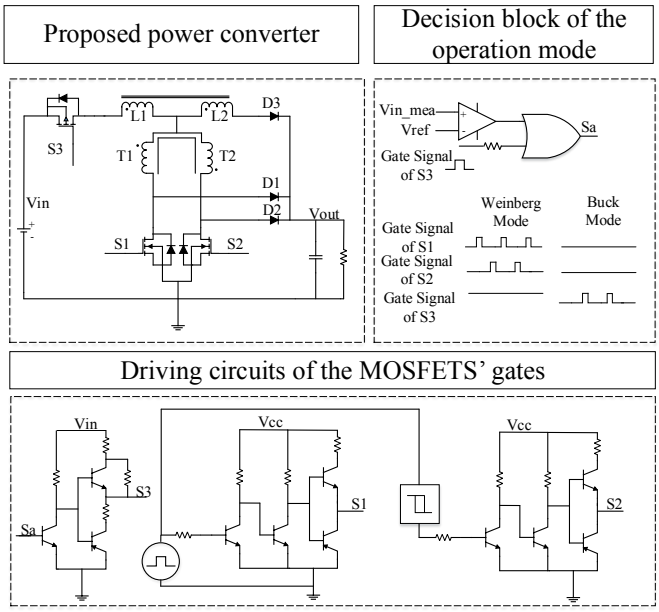

Fig. 3. The configuration of the proposed power converter and the driver circuits

When the battery voltage is smaller than the supercapacitor voltage, switch S_3 is turned on and the converter will operate as Weinberg converter and the supercapacitor voltage increases to the required level.

When S_1 (or S_2) is at on state, i_{T1} flows to ground through the coil T_1 (or T_2) of the transformer and S_1 (or S_2). The

current at the same magnitude will flow in T_2 coil ($i_{Q1}=i_{T2}$), because T_1 and T_2 have the same turns number. Since S_2 (or S_1) is at off state, i_{T2} flows through D2 to the output. The voltage at center tap of the transformer (V_{CT}) is equal to the half of the output voltage as in Eq. (1).

$$[V_{CT}]_{ON} = V_{OUT} / 2 \quad (1)$$

When the S_1 is at on state, the input current i_{L1} is equal to the sum of the currents of S_1 and D_2 and this is also valid for currents of S_2 and D_1 when S_2 is at on state. The input current i_{L1} is equal to the twice of output current as stated in Eq. (4).

$$i_{L1} = i_{S1} + i_{D2} \quad (2)$$

$$i_{S1} = i_{D2} = i_{OUT} \quad (3)$$

$$[i_{L1}]_{ON} = 2\,[i_{OUT}]_{ON} \quad (4)$$

$$V_{L1} = V_{IN} - V_{OUT}/2 = L_1\,(\Delta i_{L1} / \Delta t) \quad (5)$$

$$(\Delta i_{L1} / \Delta t)_{ON} = (V_{IN} - V_{OUT} / 2) / L_1 \quad (6)$$

$$(\Delta I_{OUT} / \Delta t)_{ON} = (1 / 2)\,(\Delta i_{L1} / \Delta t)_{ON}$$
$$= (2V_{IN} - V_{OUT}) / 4L_1 \quad (7)$$

The input current will pass through D3 when the S1 and S2 are at off state, thus input and output currents will be equal. The effective inductance is four times of the inductance of L_1 or L_2 due to the fact that their turns number is same ($N = N_{L1} = N_{L2}$).

$$L_{OFF} = (N_{L1} + N_{L2})^2\,A_L = 4\,N^2\,A_L = 4\,L_1 \quad (8)$$

$$[i_{L1}]_{OFF}\,2\,N = [i_{L1}]_{ON}\,N \quad (9)$$

$$[i_{OUT}]_{OFF} = i_{D3} = [i_{L1}]_{OFF} = 1 / 2\,[i_{L1}]_{ON} \quad (10)$$

$$(\Delta i_{L1} / \Delta t)_{OFF} = (\Delta i_{OUT} / \Delta t)_{OFF}$$
$$= (V_{IN} - V_{OUT}) / 4\,L_1 \quad (11)$$

Eq. (12) and Eq. (13) can be written considering the above given conditions.

$$V_{IN} - V_{CT} = V_{CT} - V_{OUT} \quad (12)$$

$$[V_{CT}]_{OFF} = (V_{IN} + V_{OUT}) / 2 \quad (13)$$

At steady state operation the rise and fall amplitude of i_{L1} are equal according to Eq. (4).

$$[(2V_{IN} - V_{OUT}) / 4\,L_1\,D_1] + [(1 - D_1)\,(V_{IN} - V_{OUT}) / 4\,L_1] = 0 \quad (14)$$

Eq. (15) can be obtained by simplifying Eq. (14).

$$V_{OUT} = (1 + D_1)\,V_{IN} \quad (15)$$

The small signal equation for boosting mode of the proposed hybrid converter is equal to the small signal equation of the classical Weinberg converter as in Eq. (16) [25].

$$G_{vd}(s) = \frac{V_O(s)}{d(s)} = \frac{V_{IN}}{4LCs^2 + 4\frac{L}{R}s + 1} \quad (16)$$

The stability characteristic that ensures superiority to Weinberg converter compared to classical Boost type converter is realized with the inductor and transformer combination. So it can be interpreted that the most important component of this converter is the inductor and transformer pair.

By naming battery voltage as input voltage and capacitor voltage as reference voltage throughout the explanations, when the input voltage is greater than the reference value, the power converter should operate on buck mode, so S_1 and S_2 should be at off state continuously. When S_3 is at off state, the current will flow through the body diodes of the S_1 and S_2 and L_2. When S_3 is at on state, the current will flow through L_1, T_1, T_2, D_1 and D_2. There will be no saturation problem. The proposed topology will operate as Buck converter for this condition. By taking the voltage on the input inductor as V_L, the input voltage as V_{IN}, the output voltage as V_{OUT}, the voltage on the transformer coils as V_T, the duty cycle of S3 as D_2 and the period as T, equations are obtained as stated in Eq. (17) - Eq. (19) when S1 is at on state.

$$-V_{IN} + V_L + V_T + V_{OUT} = 0 \text{ (KVL equation with the left-half of the transformer)} \quad (17)$$

$$-V_{IN} + V_L - V_T + V_{OUT} = 0 \text{ (KVL equation with the right-half of the transformer)} \quad (18)$$

$$V_L = V_{IN} - V_{OUT} \quad (19)$$

When S_3 is at off state, Eq. (20) is valid.

$$V_L = - V_{OUT} \quad (20)$$

At steady state operation Eq. (21) and Eq. (22) can be written.

$$(V_{IN} - V_{OUT})\,D_2T + (- V_{OUT})\,(T - D_2T) = 0 \quad (21)$$

$$V_{OUT} = D_2V_{IN} \quad (22)$$

Eq. (22) shows the buck operating property of the converter. The small signal equation for Buck mode of the proposed converter can be written as equal to the small signal equation of the classical Buck converter as in Eq. (23) [26].

$$G_{vd}(s) = \frac{V_O(s)}{d(s)} = \frac{V_{IN}}{LCs^2 + \frac{L}{R}s + 1} \quad (23)$$

As a result, the output voltage is D_2V_{IN} when the input voltage is greater than the reference value and $(1 + D_1)\,V_{IN}$ when the input voltage is smaller than the reference value. The proposed topology has no right half plane zero for both operation modes as it can be seen from Eq. (16) and Eq. (23). This means that there will be no instability problem. The simple approach ignoring parasitic effects is considered here while deriving the steady-state and small signal equations for both operation modes.

The driver circuits producing gate signals of MOSFETs are shown in Fig.3.

3. Results and Discussion

The results of simulation and experiments are given in this section. The simulation studies were performed using PSim and PSpice softwares to model the electronic components as quasi-real and to ensure consistency of the results with those of experiment. The parameters used for simulation and experiments are as; converter power 250 W, input voltage in range of 40-60 V, output average voltage of

50 V in the range of 48-50 V and operating frequency of 100 kHz. The hardware parameters of the prototype are given in Table 1. The hardware parameters of inductor and transformer pair which can be considered as the most important component of this converter are also given in Table 2.

Table 1. Hardware parameters of the prototype

Component	Value
Diode	V_R = 150 V, V_F = 0.71 V, I_F = 20 A
MOSFET - NMOS	V_{DSS} = 100 V, I_D = 57 A, $R_{DS\,(ON)}$ = 23 mΩ
MOSFET - PMOS	V_{DSS} = -100 V, I_D = -38 A, $R_{DS\,(ON)}$ = 60 mΩ
Transformer	L_{T1} = L_{T2} = 92 µH
Inductor	L_{L1} = L_{L2} = 8 µH
Output Capacitor	2000 µF

Table 2. Hardware parameters of the Inductor and transformer pair

	Coupled Inductor	Transformer
Number of Turns	6	4
Inductance Value	8 µH	92 µH
Current Rating (Peak)	16 A	8 A
Diameter of Cable	0.404 mm (26 AWG)	0.404 mm (26 AWG)
Number of Cables	10	10
Core Type	RM14 (gapped)	RM 14 (ungapped)
Core A_L Value	250 nH ±3%	6000 nH +30/–20%
Core Material	N87	N87

Since the proposed converter consists of one module, voltage control mode has been preferred. PI control has been chosen because of the main advantage of this controller is its ability to ensure zero steady-state error under disturbances as long as the closed-loop system is stable [27]. The supercapacitor voltage is controlled using PI control method and the coefficients of controller were derived using PID Tuner Toolbox of MATLAB software. The corresponding coefficients are given in Table 3.

Table 3. Control Coefficients of the Proposed Circuit

Coefficient	Value
Kp (for Buck mode)	9.2
Ki (for Buck mode)	33334
Kp (for Weinberg mode)	0.1
Ki (for Weinberg mode)	316

The effect of the load changes on the converter parameters as input voltage and supercapacitor voltage, battery current, supercacitor current are analyzed. For this purpose, the SAR load changes from full load to zero and vice versa. The effect of these changes is investigated. The responses of the above mentioned parameters corresponding to input voltage of V_{in} = 60 V (Buck mode) and V_{in} = 40 V (Weinberg mode) are shown in Fig. 4 and Fig. 5, respectively. It is shown from the figure that when SAR load is activated or deactivated, the battery current doesn't change considerably while supercapacitor meets almost all the changes in the load current.

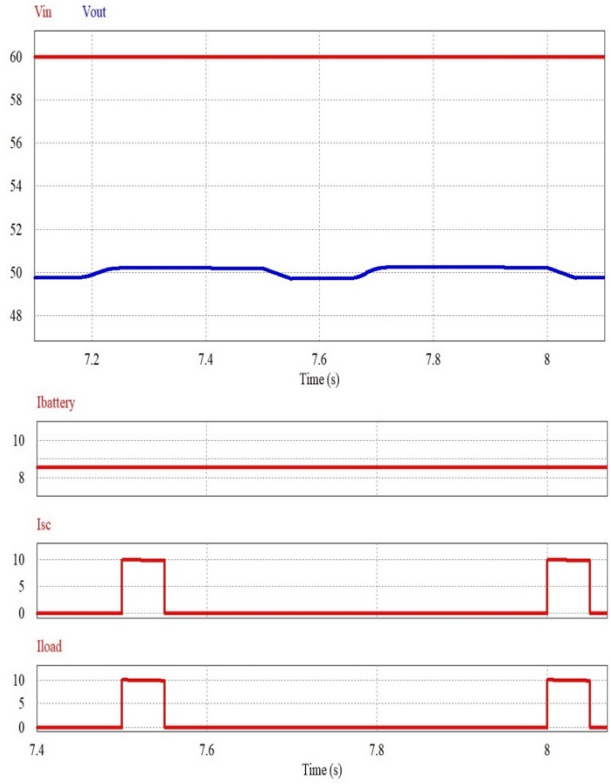

Fig. 4. Response of converter parameters to a pulse load change, V_{in} = 60 V (Buck Mode)

The response waveforms of V_{in}, V_{out}, I_{L1}, I_{L2}, gate signals of S_1, S_2 and S_3 are shown in Fig. 6 for Buck mode and in Fig. 7 for Weinberg mode operation. When the input voltage is greater than the supercapacitor voltage S_1 and S_2 are at off state and S_3 is switching so that the converter operates at Buck mode operation to decrease the input voltage matching with the supercapacitor voltage. When the input voltage is lower than the supercapacitor voltage, S_3 is at off state and S_1 and S_2 are switching and the converter operates at Weinberg mode operation.

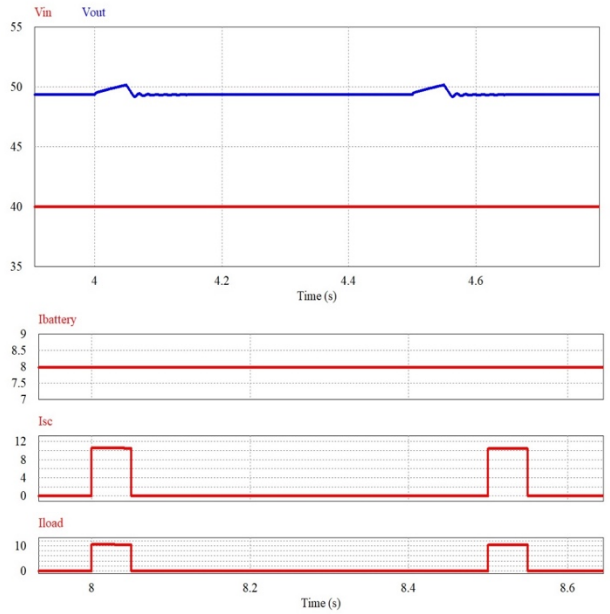

Fig. 5. Response of converter parameters to a pulse load change, V_{in} = 40 V (Weinberg Mode)

The response waveforms of V_{in}, V_{out}, I_{L1}, I_{L2}, gate signals of S_1, S_2 and S_3 are shown in Fig. 6 for Buck mode and in Fig. 7 for Weinberg mode operation. When the input voltage is greater than the supercapacitor voltage S_1 and S_2 are at off state and S_3 is switching so that the converter operates at Buck mode operation to decrease the input voltage matching with the supercapacitor voltage. When the input voltage is lower than the supercapacitor voltage, S_3 is at off state and S_1 and S_2 are switching and the converter operates at Weinberg mode operation.

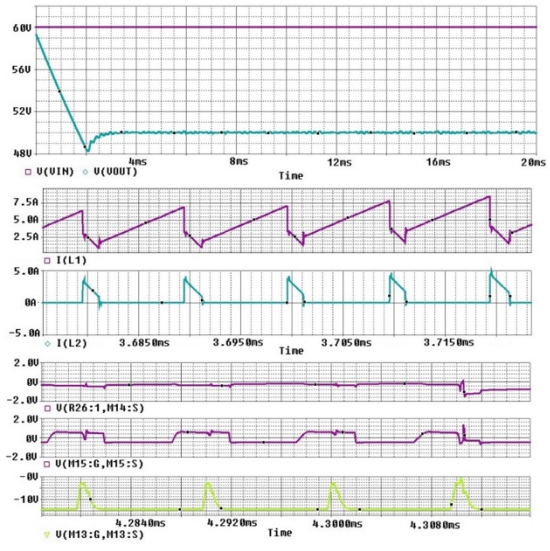

Fig. 6. Waveforms of V_{in}, V_{out}, I_{L1}, I_{L2}, gate signals of S_1, S_2 and S_3 for V_{in} = 60 V (Buck mode – load is constant and equal to 250 W)

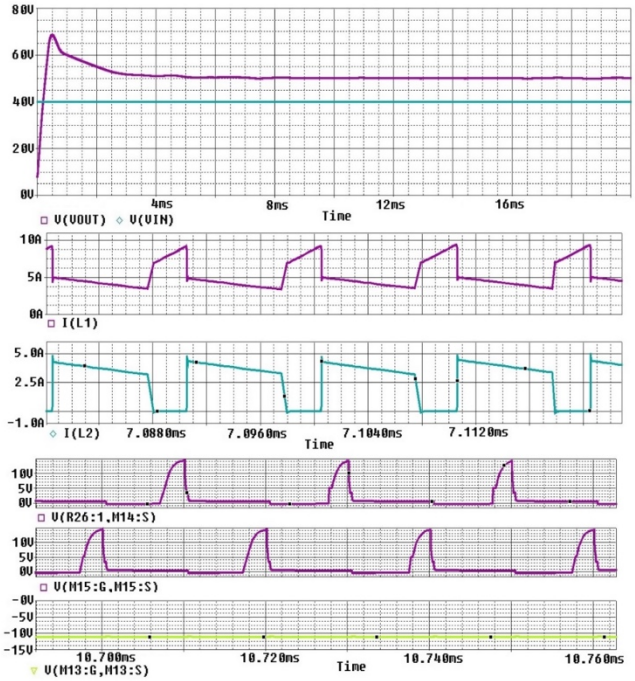

Fig. 7. Waveforms of V_{in}, V_{out}, I_{L1}, I_{L2}, gate signals of S_1, S_2 and S_3 for V_{in} = 40 V (Weinberg mode – load is constant and equal to 250 W)

The effect of load changes on the converter parameters for Buck mode operation is shown in Fig. 8. For this case, the load increases in step form from 125 W to 250 W at the time instant of 16 ms. It is shown in the figure that the control unit operates accurately to keep the capacitor voltage at the reference value of 50 V.

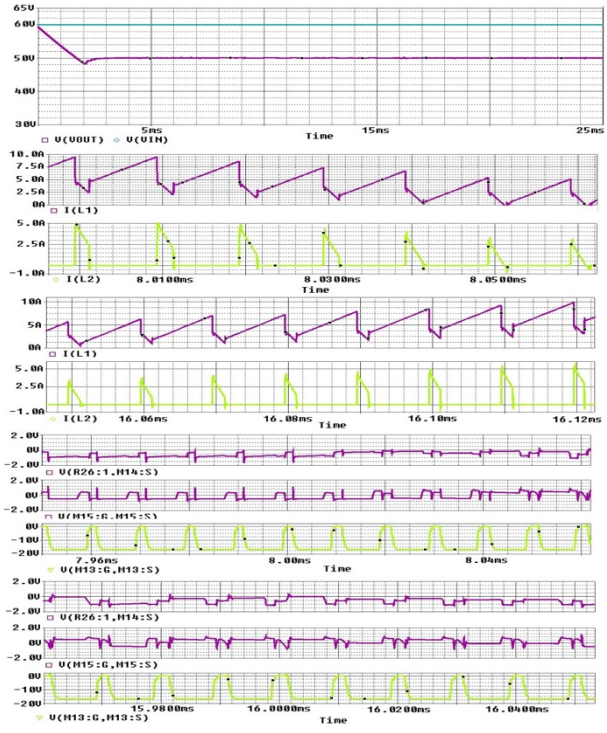

Fig. 8. Waveforms of V_{in}, V_{out}, I_{L1}, I_{L2}, gate signals of S_1, S_2 and S_3 for V_{in} = 60 V (Buck mode – load decreases from 250 to 125 W at the time stand of 8ms and increases from 125 to 250 W at instant of 16 ms)

Figures 9 and 10 are experimental results corresponding to input and output voltages and the gate signals of the converter switches. As it is shown, only S_3 is operating and S_1 and S_2 are at off state and converter is operating at Buck mode operation.

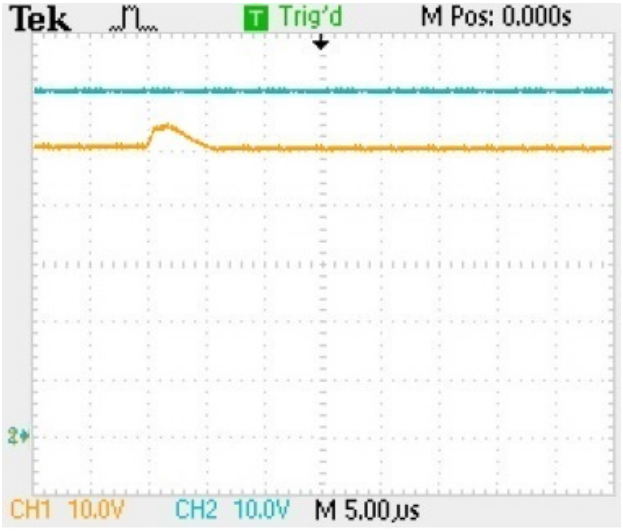

Fig. 9. Input (upper) and output (lower) for V_{in} = 60 V (Buck mode – controlled version / load transition)

Fig. 10. Input (upper) and output (lower) for V_{in} = 60 V (Buck mode – controlled version / load transition)

The waveforms of the converter parameters corresponding to the case where converter is operating in Weinberg mode operation are shown in Fig. 11. In this operation the load power decreases from 250 W to 125 W at the time stand of 8 ms and then it increases to 250 W at the time instant of 16 ms. It is shown that the converter and the control system operate accurately and the capacitor voltage remains constant at the reference voltage as 50 V.

The experimental results corresponding to input, output voltages and the gate signals of the converter switches are shown in Fig. 12 and Fig. 13, respectively. As it is shown, only S_3 is at on state continuously and S_1 and S_2 are switching and converter is operating at Weinberg mode operation.

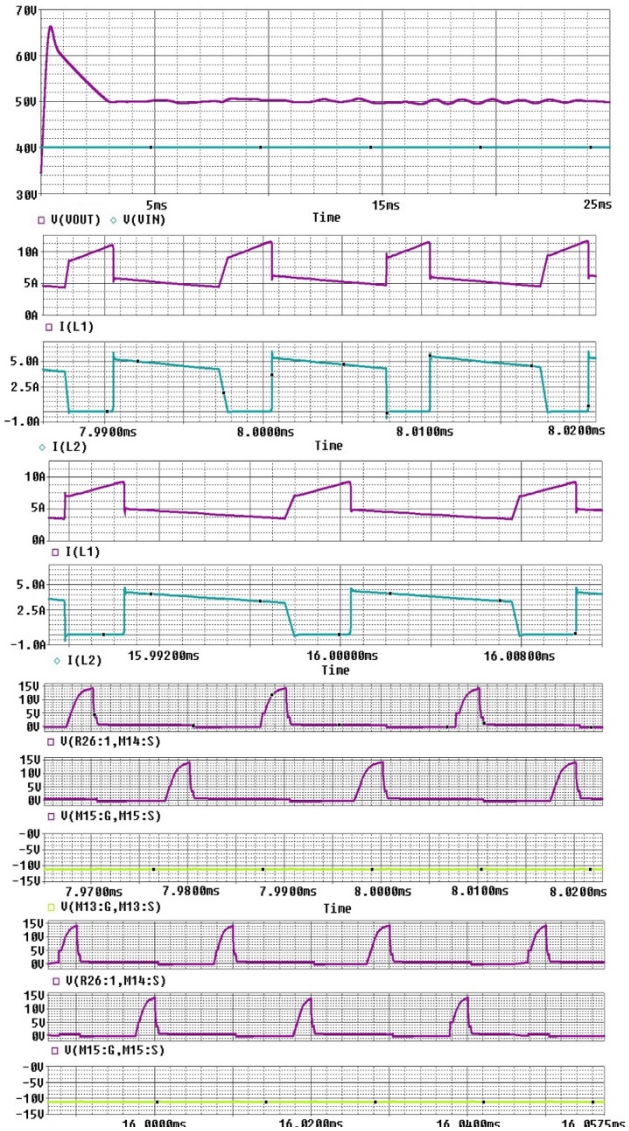

Fig. 11. Waveforms of V_{in}, V_{out}, I_{L1}, I_{L2}, gate signals of S_1, S_2 and S_3 for V_{in} = 40 V (Weinberg Mode – load decreases from 250 to 125 W at the time stand of 8ms and increases from 125 to 250 W at instant of 16 ms)

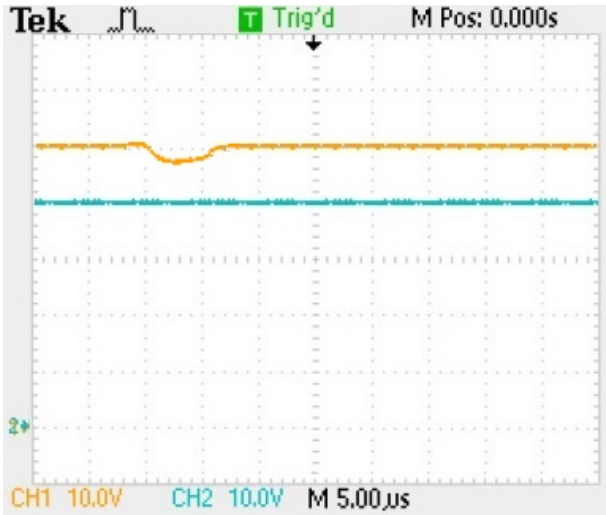

Fig. 12. Input (upper) and output (lower) for V_{in} = 40 V (Weinberg mode – controlled version / load transition)

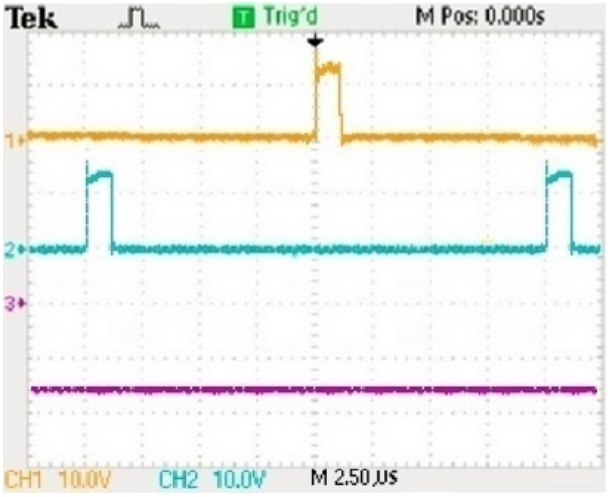

Fig. 13. Gate signals of S_1, S_2 and S_3 for V_{in} = 40 V (Weinberg mode – controlled version / load transition)

The waveforms of the converter parameters corresponding to case of transition from Buck to Weinberg mode are shown in Fig. 14. Firstly, the input voltage is greater than capacitor voltage and converter is operating in Buck mode operation and at the time instant of 8 ms the input voltage suddenly decreases to 40 V (lower than capacitor voltage) causing a transition from Buck to Weinberg mode operation. For this case of operation, the converter is supplying full load of 250 W. The experimental results corresponding to input and capacitor voltage and gate signals of S_1, S_2, and S_3 for this transition are shown in Fig. 15 and Fig. 16, respectively.

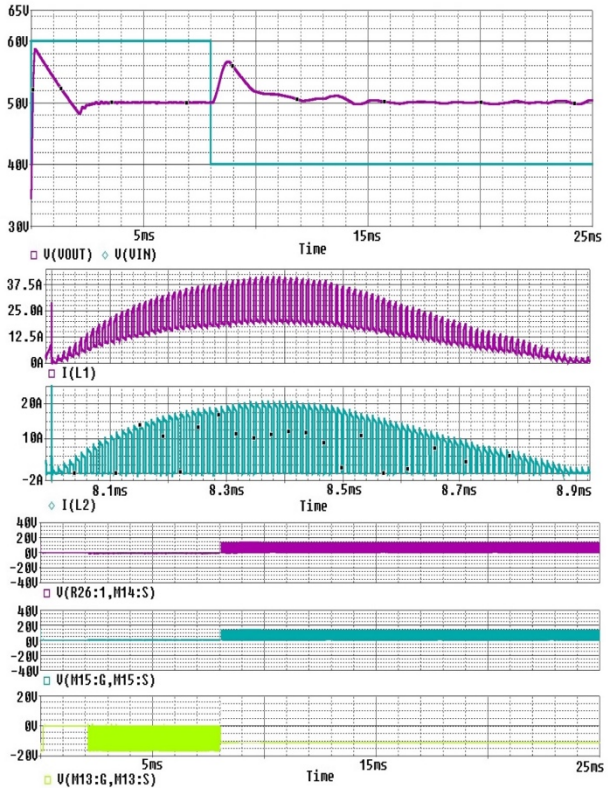

Fig. 14. Waveforms of V_{in}, V_{out} and gate signals of S_1, S_2 and S_3 for the case of transition of converter from Buck to Weinberg operation mode at instant of 8ms

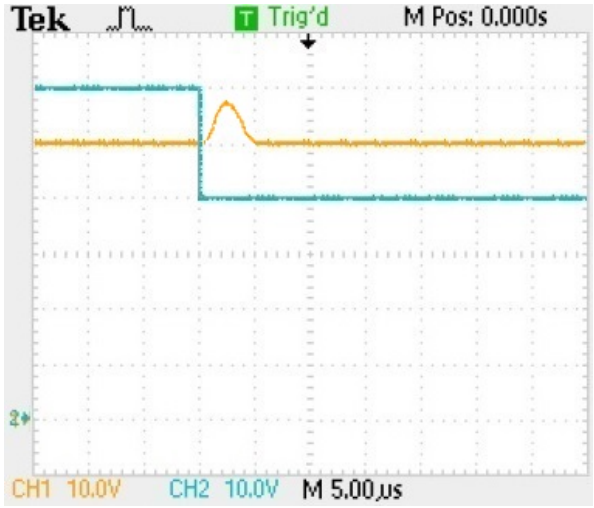

Fig. 15. Input and output Signals for input transition (from Buck Mode to Weinberg Mode) (Green signal is input voltage and orange signal is output voltage.)

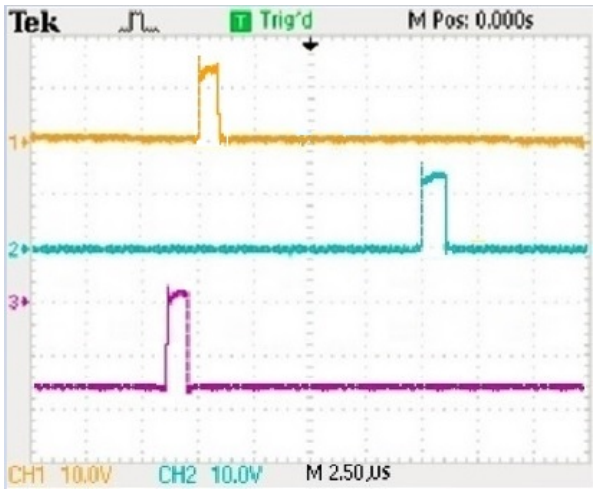

Fig. 16. Gate signals of S_1, S_2 and S_3 for transition from Buck to Weinberg Mode

Investigating the simulation and experimental results shows that they seem to be very consistent. The output voltage is settled to target value (50 V) for both operation modes and transition conditions and output voltage value is in the expected ranges of 50 ± 2 V.

The stability of the proposed converter is investigated by drawing Bode diagrams according to operation modes using MATLAB software. For compensated conditions, the crossover frequency is 7.36 KHz and the phase margin is 74.1° for Buck mode, and the corresponding parameters for Weinberg mode operation are 2.42 KHz and 74°, respectively. These values are much better than the values given in [22] as the minimum acceptable values. The Bode diagrams of the proposed converter corresponding to Buck and Weinberg mode operations are given in Fig. 17 and Fig. 18, respectively. It is shown that there is no stability problem considering the related diagrams if control coefficients is tuned properly.

It is intended to keep the capacitor voltage in a safe region to supply the SAR load against different conditions as voltage changes in the input. For this purpose, classical

converters of Buck and Weinberg can be used separately considering the stability property of these converters. The converter proposed in this study combines the properties of the Buck and Weinberg converters and in addition to these, the number of elements used in this converter is lower than number of elements used in two separate Buck and Weinberg converters and this provides significant advantages to the proposed converter such as efficiency, small volume and weight, lower cost, and etc.. Some properties of the proposed converter, classical Weinberg and Buck converters are compared in Table-5.

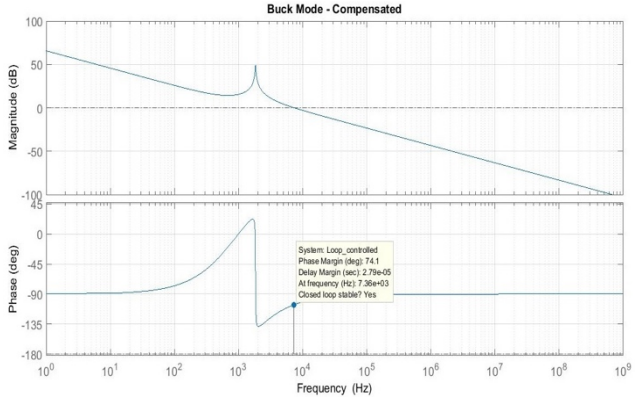

Fig. 17. Bode graph for compensated conditions (for Buck mode operation)

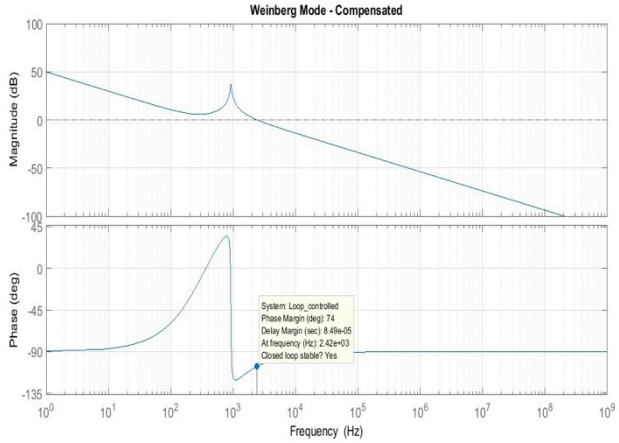

Fig. 18. Bode Graph for Compensated Conditions (for Weinberg mode operation)

Table 5. Comparison of the cited converters

	Classical Weinberg Converter	**Classical Buck Converter**	**The Proposed Converter**
Effect on Input Voltage	Only increase	Only decrease	Increase-Decrease
Stability	+	+	+
Operating Frequency	✓✓	✓	✓✓
Number of Components In Power Stage	9	5	10

4. Conclusion

In the scope of this study, a new power converter topology feeding supercapacitor from battery was designed to improve the life expectancy of battery and respond to instantaneous power changes of SAR satellites. The life of the battery and consequently the life of the satellite will be extended by ensuring the instantaneous power need by means of supercapacitor instead of the battery. The proposed power converter will be placed between the battery and the supercapacitor. The capacitor voltage is controlled by the proposed converter to remain in the safe region against different voltage levels of the batteries. There is no instability problem because of the absence of the right half plane zero for both operation modes ensuring the stability of the converter during tuning control coefficients properly. In addition, the proposed converter has advantages over using two separate classical Buck and Weinberg converters considering number of circuit element, weight, volume, cost, efficiency, etc. Moreover, the proposed converter has the property of controlling the capacitor voltage in the wide range between D_2 V_{IN} and (1 + D_1) V_{IN}. Theoretical, simulation and experimental results are consistent with each other and the theoretical study carried out in this work is verified by the results of simulation and experiments.

References

[1] D. Cohen, Y. C. Eldar, "Sub-Nyquist radar systems: temporal, spectral, and spatial compression", IEEE Signal Processing Magazine, DOI: 10.1109/MSP.2018.2868137, Vol: 35 , No: 6 , pp. 35-58, November 2018. (Article)

[2] Y. Kalkan, "Frequency-only radars and other frequency-based systems with applications", IEEE Microwave Magazine, DOI: 10.1109/MMM.2016.2541821, Vol: 17, No: 7 , pp. 26-52, June 2016. (Article)

[3] T. Sakagami, Y. Shimizu, H. Kitano, "Exchangeable batteries for micro EVs and renewable energy", 6th International Conference on Renewable Energy Research and Applications, San Diego, CA, USA, pp. 701 – 705, 5-8 November 2017. (Conference Paper)

[4] M. M. G. Lawan, J. Raharijaona, M.B. Camara, B. Dakyo, "Power control for decentralized energy production system based on the renewable energies — using battery to compensate the wind/load/PV power fluctuations", 2017 IEEE 6th International Conference on Renewable Energy Research and Applications (ICRERA), San Diego, CA, USA, pp. 1132 – 1138, 5-8 November 2017. (Conference Paper)

[5] A. Harrouz, M. Abbes, I. Colak, K. Kayisli, "Smart grid and renewable energy in Algeria", 2017 IEEE 6th International Conference on Renewable Energy Research and Applications (ICRERA), San Diego, CA, USA, pp. 1166 – 1171, 5-8 November 2017. (Conference Paper)

[6] D. Motyka, M. Kajanová, P. Braciník, "The impact of embedded generation on distribution grid operation", 2018 7th International Conference on Renewable Energy

Research and Applications (ICRERA), Paris, France, pp. 360 – 364, 14-17 October 2018. (Conference Paper)

[7] P. Mazidi, G. N. Baltas, M. Eliassi, P. Rodríguez, "A model for flexibility analysis of RESS with electric energy storage and reserve", 2018 7th International Conference on Renewable Energy Research and Applications (ICRERA), Paris, France, pp. 360 – 364, 14-17 October 2018. (Conference Paper)

[8] Y. Chang, H. Fang, Y. Zhang, "A new hybrid method for the prediction of the remaining useful life of a lithium-ion battery", Applied Energy, DOI: 10.1016/j.apenergy.2017.09.106, Vol: 206, No: 1, pp. 1564 – 1578, September 2017. (Article)

[9] A. Maddu, A. Saputra, N. I. Ayuningtiyas, A. Tsalsabila, A. Ismayana, N. Nurhalim, S. Arjo, "Synthesis of MnO_2/Carbon Dots Nanocomposite Derived From Rice Husk for Supercapacitor Electrodes", International Journal of Renewable Energy Research, Vol: 8, No: 3, pp. 1476 – 1482, September 2018. (Article)

[10] S. J. A. D. Hosseini, M. Moazzami, H. Shahinzadeh, "Optimal sizing of an isolated hybrid wind/PV/battery system with considering loss of power supply probability", Majlesi Journal of Electrical Engineering, Vol: 11, No: 3, September 2017. (Article)

[11] Y. Gaurav, C.K. Gowrishankara, V.K. Hariharan, "Analysis and development of Weinberg converter with fault tolerant feature", Biennial lnternational Conference on Power and Energy Systems: Towards Sustainable Energy (PESTSE), Bangalore, India, 21-23 Jan. 2016. (Conference Paper)

[12] N. M. Ibrahim, J. V. Gangadhar, M. Partho, K. Deepa, "High frequency SEPIC-WEIBERG converter for space applications", International Conference on Inventive Computation Technologies (ICICT), Coimbatore, India, 26-27 Aug. 2016. (Conference Paper)

[13] M. Fu, D. Zhang, T. Li, Y. Li, "High direction-changing frequency bidirectional DC-DC converter for charging/discharging applications", IECON 2017 - 43rd Annual Conference of the IEEE Industrial Electronics Society, Beijing, China, pp. 4375 – 4382, 29 Oct.-1 Nov. 2017. (Conference Paper)

[14] Q. Chen, P. Qiu, Y. Lu, "Power loss and efficiency analysis of non-isolated weinberg converter", IECON 2017 - 43rd Annual Conference of the IEEE Industrial Electronics Society, Beijing, China, pp. 4443 – 4448, 29 Oct.-1 Nov. 2017. (Conference Paper)

[15] Q. Tong, H. Zhang, D. Zhang, "A ZVS and ZCS DC-DC converter based on weinberg topology for high voltage applications", 13th IEEE Conference on Industrial Electronics and Applications (ICIEA), Wuhan, China, pp. 177 – 200, 31 May-2 June 2018. (Conference Paper)

[16] J. G. Llorente, A. R. Vecino, L. A. G. Rodriguez, J. C. Balda, E. I. O. Rivera, "Simple and efficient low power photovoltaic emulator for evaluation of power conditioning systems", 2016 IEEE Applied Power Electronics Conference and Exposition (APEC), Long Beach, CA, USA, pp. 3712 – 3716, 20-24 March 2016. (Conference Paper)

[17] G. D. Capua, N. Femia, K. Stoyka, "Power magnetics volume and weight reduction in aerospace power supply units", IEEE 17th Workshop on Control and Modeling for Power Electronics (COMPEL), Trondheim, Norway, 27-30 June 2016. (Conference Paper)

[18] C. Armbruster, C. Schoener, T. Schoenbett, A. Kloenne, R. Merz, "Development of a high efficient MPPT for space applications using GaN power transistors", PCIM Europe 2017, International Exhibition and Conference for Power Electronics, Intelligent Motion, Renewable Energy and Energy Management, Nuremberg, Germany, pp. 451 - 456, 16-18 May 2017. (Conference Paper)

[19] B. Tulsyan, , M. M. Zaheer, "Maximum power point tracking based solar charge regulator", International Conference on Computational and Characterization Techniques in Engineering & Sciences (CCTES), Lucknow, India, India, pp. 71 - 76, 14-15 Sept. 2018. (Conference Paper)

[20] A. Sun, W. Zhang, X. Lin, J. Li, "Modeling and stability analysis of high voltage ratio bidirectional DC/DC converter applied to electric vehicle", IEEE Conference and Expo Transportation Electrification Asia-Pacific (ITEC Asia-Pacific), Beijing, China, pp. 1 - 6, 31 Aug.-3 Sept. 2014. (Conference Paper)

[21] AIAA S-122-2007, Electrical Power Systems for Unmanned Spacecraft, American Institute of Aeronautics and Astronautics, 2007. (Standards and Reports)

[22] ECSS-E-ST-60-10C, Space engineering-Control performance, European Cooperation for Space Standardization, 2008. (Standards and Reports)

[23] S. Arora, P. Balsara, D. Bhatia, "Input–output linearization of a Boost converter with mixed load (Constant voltage load and constant power load)", IEEE Transactions on Power Electronics, DOI: 10.1109/TPEL.2018.2813324, Vol: 34, No: 1, pp. 815 – 825, January 2019. (Article

[24] S. Bose, Y. V. Hote, S. D.Hanwate, "Analysis of effects due to right half plane zeros in PI controller based hydro turbine", 2018 IFAC (International Federation of Automatic Control) Hosting by Elsevier Ltd., DOI: 10.1016/j.ifacol.2018.06.167, Vol: 51, No: 4, pp. 633 – 638, June 2018. (Article)

[25] L. Weijun, L. Yanjun, "Small signal modeling and analysis of the Weinberg converter for high-power satellites bus application", Chinese Journal of Electronics, vol. 18, no. 1, pp. 171-176, 2009. (Article)

[26] Robert W. Erickson, Dragan Maksimovic, Fundamentals of Power Electronics, 2nd ed., vol. 2. KLUWER ACADEMIC PUBLISHERS, 2004, pp.293-302. (Book)

[27] G. Tulay, İ. İskender, H. Erdem, "Optimal tuning of a Boost PFC converter PI controller using heuristic optimization methods", International Transactions on Electrical Energy Systems, DOI: 10.1002/etep.2458, vol. 27, no. 12, pp. 1-10, 2017. (Article)